

Internal tides and baroclinicity in the Southern Weddell Sea 2. Effects of the critical latitude and stratification

Robin Robertson

Lamont-Doherty Earth Observatory, Columbia University, Palisades, New York, USA

Abstract. Tidal dynamics affect Antarctic Bottom Water and Ice Shelf Water production in the southern Weddell Sea and the general circulation and mixing. In this region, tidal dynamics were found to be extremely sensitive both to the proximity of the continental shelf-slope break to the critical latitude ψ_{crit} and to the existence of a shelf break front. If the continental slope was not in the vicinity of ψ_{crit} or a shelf break front was absent, generation of internal tides was negligible. Generation of internal tides was greatest when both a shelf break front was present and the continental slope was near and equatorward of ψ_{crit} . When a shelf break front was present and the continental slope was near but poleward of ψ_{crit} , a strong benthic response occurred. This response included development of benthic inertial oscillations at the continental shelf-slope break, increased benthic shear, a thicker benthic boundary layer, and increased benthic dissipation. A shelf break front with even a slight horizontal density gradient was found to significantly enhance internal tide generation and/or the benthic effects.

1. Introduction

Tidal dynamics influence mixing both through shear instabilities from internal tides and through benthic stress associated with barotropic or baroclinic tidal velocities. The motivation for investigation of the internal tides, baroclinicity, and tidal mixing in the Weddell Sea was discussed in a companion paper [Robertson, this issue] (hereafter referred to as part 1). The Princeton Ocean Model (POM) was used to investigate internal tides and tidal dynamics in the southern Weddell Sea. Part 1 of this investigation described the numerical model and showed that the modeled cross-slope velocities agreed well with the existing observations.

Tidal dynamics, particularly the generation and propagation of internal tides, are highly dependent on many factors, including topography, stratification, and proximity to the critical latitude ψ_{crit} which is the latitude where the inertial frequency equals the tidal frequency. Linear internal wave theory predicts that ψ_{crit} and stratification affect the regions of generation and propagation of internal tides. Internal tides will neither be generated nor will they propagate poleward of ψ_{crit} . Weaker stratification is associated with weaker internal tidal generation, slower group velocities, and steeper internal wave ray characteristics. (For a more in depth explanation of linear internal wave theory, see part 1, section 3.) In addition, Furevik and Foldvik [1996] noted that ψ_{crit} affects the benthic boundary layer with the benthic boundary layer thickness increasing near ψ_{crit} .

In order to investigate the dependence of the tidal dynamics on these three factors a sensitivity study was undertaken. The effects of ψ_{crit} on the tidal dynamics are described in section 2. The sensitivity of the internal tidal fields to stratification and topography are investigated in sections 3 and 4, respectively. Section 5 discusses the implications of the model results. A summary is provided in section 6.

2. Critical Latitude Effects

2.1. Transect A Without the Critical Latitude

To evaluate the effects of ψ_{crit} , two scenarios were used: one without and one with ψ_{crit} (transect A in Figure 1) in the domain. For the case without ψ_{crit} the latitude of the domain was altered 10° to the north so that ψ_{crit} did not fall within the domain. The amplitude of the M_2 tidal elevations η without ψ_{crit} ranged from 0.44 m at the deep water end to 0.50 m at the ice shelf end (solid line in Figure 2a), and the phase remained relatively constant over the transect at $\sim 292^\circ$ (not shown). The major axes for the depth-independent velocities for the M_2

constituent (solid line in Figure 2b) were strongly influenced by the topography (shaded line in Figure 2b) increasing dramatically over the outer continental shelf and under the ice shelf.

As predicted by linear theory (part 1, Figure 5a), essentially no internal tides were generated when ψ_{crit} was not in the domain (Figure 3a). In these conditions, an extremely slight internal tide occurred near the surface over the continental slope and was evident both in the cross-slope velocity profiles at a time near the peak onshore depth-independent tidal flow ($t = 45.625$ days) (t is the time since the start of the simulation) (Figure 3a) and in the major axes of the tidal ellipses (Figure 4a) by the divergence and convergence of the profiles and the alternating areas of low and high major axes, respectively. Since the internal tidal response was essentially negligible, the depth dependence of the cross-slope velocity consisted primarily of ice shelf and benthic boundary layers. A ~ 50 m thick benthic boundary layer was apparent in the profiles of the cross-slope depth-dependent velocities over the upper continental slope (Figure 3a). The POM-generated vertical viscosity K_M was in the range of 10^{-2} to 10^{-6} $\text{m}^2 \text{s}^{-1}$.

2.2. Critical Latitude Effects in a Stratified Ocean

To investigate the effect of ψ_{crit} , the former simulation was compared to one with ψ_{crit} in the domain (Figure 1). The amplitudes of the elevation for simulations with M_2 forcing without ψ_{crit} passing through the domain (solid line in Figure 2a) increased over the continental shelf and slope, whereas those with ψ_{crit} (dashed line in Figure 2a) were constant over nearly the entire transect. This difference between the elevation amplitudes for the two simulations reached 5 cm at the front of the ice shelf. This difference in behavior (solid and dashed lines in Figure 2a, respectively) is attributed to the blockage of a southward propagating Poincaré wave. Theoretically, Poincaré waves cannot propagate poleward of ψ_{crit} . Therefore, in the case with ψ_{crit} in the domain, southward propagating Poincaré waves are blocked and do not propagate onto the continental shelf. The amplitude remained constant in the domain (dashed line in Figure 2a) since the Poincaré forcing wave propagates primarily westward along the slope. When ψ_{crit} was absent, the elevation amplitude increased over the continental shelf, reflecting the southward propagation of Poincaré waves into shallower water (solid line in Figure 2a).

The major axes of the depth-independent velocities were slightly smaller over the continental shelf than those of the simulation without ψ_{crit} (Figure 2b). Again, the decreased amplitude with ψ_{crit} is attributed to blockage of southward propagating Poincaré waves. There was slightly more kinetic and potential energy in the “barotropic mode” of the model simulation when ψ_{crit} was absent, particularly over the continental shelf poleward of ψ_{crit} .

There was more energy in the “baroclinic mode” of the model simulation when ψ_{crit} was present. The increase in baroclinic energy was apparent both in the profiles of the cross-slope depth-dependent velocity (Figure 3) and in the major axes of the tidal ellipses for the depth-dependent velocities (Figure 4). (The major axes of the tidal ellipses over the entire transect for the simulation when ψ_{crit} was present are shown in part 1, Figure 9.) The profiles of the cross-slope velocities showed much more vertical variation over the upper continental slope with ψ_{crit} in the domain (Figure 3b) than without (Figure 3a). Strong vertical shears occurred from ~ 500 to 600 km along the transect in the region of the shelf break front (Figure 3b). In this scenario, much of the critical γ region, where internal tides are predicted by linear internal wave theory, coincided with the location of the shelf break front. Although the effects of the stratification, specifically the shelf break front, and ψ_{crit} were intertwined, an effort will be made to separate the effects and to focus on ψ_{crit} effects in this section and stratification effects in section 3. Some convergence and divergence of the cross-slope velocity profiles occurred near the surface (Figure 3b), indicating equatorward propagation of internal tides. Although the profiles were just a snapshot in time and could not verify that these motions were internal tides, similar observations made in the major axes for the tidal ellipses confirmed their oscillatory nature (Figure 4b). However, any phase information such as the phase shift in the vertical direction apparent in the snapshot (Figure 3b) was lost with the major axes of the tidal ellipses. Still, the major axes showed more vertical variation with ψ_{crit} in the domain (Figure 4b) than without (Figure 4a), and the most vertical variation occurred equatorward of ψ_{crit} in the region of the shelf break front. Additionally with ψ_{crit} , higher velocities at the tidal frequency occurred in the lower water column over the upper continental slope (Figure 4b). The location of the vertical variation associated with ψ_{crit} , the wavelength of ~ 70 - 90 km, and the phase speed of ~ 0.04 m s^{-1} taken from time-cross-slope distance plots (not shown) were consistent with internal tidal dynamics.

2.3. Critical Latitude Effects in a Homogeneous Ocean

Comparing simulations for transect A with a homogeneous ocean (defined as a constant θ and S over the entire domain) and with or without ψ_{crit} in the domain showed there to be more “baroclinic mode” kinetic energy with ψ_{crit} in the domain and more “barotropic mode” potential and kinetic energy without, similar to the results for the corresponding stratified cases. The “barotropic mode” results were essentially indistinguishable from

those shown in Figure 2 for the respective stratified simulations. Since internal waves do not exist in a homogeneous ocean, the “baroclinic mode” energy was associated with the boundary layers. Over the outer continental shelf and slope the benthic boundary layer was of interest since there was no ice shelf in this region. Profiles of the cross-slope velocity at a time near the peak onshore flow ($t = 45.625$ days) showed a benthic boundary layer extending from the bottom to the surface when ψ_{crit} was in the domain (dashed line in Figure 5). A thinner benthic boundary layer, <100 m thick, existed when ψ_{crit} was not in the domain (solid line in Figure 5). ψ_{crit} effectively increases the benthic boundary layer thickness, as discussed in part 1, section 3.3.

Following the formulation of *Furevik and Foldvik* [1996] and using a $K_M = 0.005 \text{ m}^2 \text{ s}^{-1}$ (typical for this location and stratification), a benthic boundary layer thickness of ~ 70 m was estimated when ψ_{crit} was absent. This agreed with the benthic boundary layer thickness of the model. Using this formulation and K_M for a simulation with ψ_{crit} , a benthic boundary layer thickness of ~ 390 m was estimated near ψ_{crit} . This boundary layer would encompass nearly the entire water column. It should be noted that the theory assumed a constant K_M , whereas the model used a variable K_M .

2.4. Effect of the Location of the Critical Latitude

To investigate the effect of the location of ψ_{crit} on the vertical structure of the horizontal velocities, the latitude for the domain was altered so the location of ψ_{crit} varied from the midcontinental shelf to the lower continental slope (Figure 6). Since the real topography was complicated, an idealized version of the topography, which approximated the slope steepness of the real transect, was used. This idealized topography was determined using *Saint Guily's* [1976] model with *Middleton et al.'s* [1987] parameterization. This parameterization specified the offshore distance y and depth h in terms of an independent parameter q according to

$$\begin{aligned} h &= h_{\text{off}} + h_o (1 + \lambda \tanh q) \\ y &= y_{\text{off}} + a [1 + q + \lambda \ln (\cosh q)]; \end{aligned} \quad (1)$$

where a was the slope scale width, λ was a steepness parameter, h_o was a depth scaling factor, and y_{off} and h_{off} were offsets used to match the general topographic profile for the distance and depth, respectively. The values for these parameters for the idealized slope were $a = 98.9$ km, $h_{\text{off}} = -75$ m, $h_o = 2198$ m, $\lambda = 0.827$, and $y_{\text{off}} = 520$ km.

When ψ_{crit} was located in the middle of the continental shelf, internal tides were generated at the continental shelf-slope break and propagated both poleward and equatorward in the surface layer, as seen in major axes of the tidal ellipses (Figure 6a). The strongest vertical variation in the major axes appears at the continental shelf break in the region of the shelf break front ($y = 500$ - 580 km). When ψ_{crit} was located over the continental shelf-slope break, internal tidal velocities were larger deeper in the water column (Figure 6b) than when ψ_{crit} was located on the continental shelf (Figure 6a). Again, most of the vertical variation in the major axes occurred at the continental shelf break in the region of the shelf break front. For both of these simulations the peaks in the major axes were aligned with the internal wave characteristics (part 1, Figure 6a). The propagation of the internal tide was primarily in the equatorward direction (Figure 6b) when ψ_{crit} was located on the continental shelf-slope break. However, when ψ_{crit} was located on the shelf, some poleward propagation occurred (Figure 6a), as seen by the bands of higher and lower amplitudes in the major axes. When ψ_{crit} was located over the middle or lower continental slope, internal tide generation and the vertical variation in the horizontal velocities were reduced (Figures 6c and 6d). Some vertical structure in the major axes did appear in the region of the front ($y = 500$ - 580 km), with less vertical structure when ψ_{crit} was located farther down the continental slope (Figures 6c and 6d). The most striking feature was the development of a near-bottom jet, which oscillated at the tidal frequency. This near-bottom jet was a set of inertial oscillations. For both of these simulations ψ_{crit} was equatorward of the continental shelf-slope break; therefore linear theory predicts neither the generation or the existence of internal tides here. Thus the vertical variation of the major axes was not attributable to internal tides. Although it is possible that the near-bottom oscillating jet was leakage of internal tides due to their long wavelengths (~ 80 km) or internal tides advected into this area, it is more likely to be an inertial oscillation. This inertial oscillation developed because of interactions of the barotropic tide with the topography and the shelf break front in the vicinity of ψ_{crit} . Since the area was near ψ_{crit} , the forcing of the barotropic tide induced inertial oscillations, resonant effects enhanced this inertial oscillation, and advection and diffusion spread them both horizontally and vertically through the water column. As the distance from ψ_{crit} increased, the resonance between the tide and the inertial frequency diminished, as did the near-bottom jet. There was also change in the benthic boundary layer, which increased both in the vicinity of ψ_{crit} and over the upper continental shelf.

In summary, the generation of internal tides was enhanced when ψ_{crit} was poleward of the continental shelf break, and the most generation occurred when ψ_{crit} was located near the outer continental shelf or the continental

shelf-slope break When ψ_{crit} was equatorward of the continental shelf break, there was a strong benthic response in the form of a thick benthic boundary layer and less generation of internal tides.

3. Stratification Effects

3.1. Effect of a Shelf Break Front

A front has the capability to reflect or absorb wave energy, thereby dissipating internal wave energy [Baines, 1986]. The standard stratification included an idealized shelf break front from $y = 500\text{-}580$ km (part 1, Figure 1) and is described in full in part 1, section 2.2. In this front the changes in θ and S compensate for each other, and there was essentially no horizontal potential density gradient over most of the water column. This compensation was not perfect, and a slight horizontal density gradient ($< 8 \times 10^{-7} \text{ kg m}^{-4}$) existed below 300 m between 530 and 580 km. This horizontal density gradient was weaker than those (typically $1\text{-}2 \times 10^{-6} \text{ kg m}^{-4}$) of shelf break fronts observed in this region during Ice Station Weddell [Huber *et al.*, 1994].

To investigate the effect of the shelf break front, a simulation was performed using the deep water stratification over the entire domain. Although there was essentially no change in the depth-independent velocities (not shown), the vertical variation in the depth-dependent horizontal velocities was drastically reduced with the absence of the shelf break front. The major axes of the tidal ellipses without the shelf break front (Figure 7a) were nearly uniform with depth compared to those with the shelf break front (Figure 4b). The profiles of the cross-slope velocity at a time near the peak onshore flow ($t = 45.625$ days) also showed that most of the vertical variation occurred in the a benthic boundary layer (Figure 8a).

Thus the behavior of the depth-dependent velocities differed with the presence of a shelf break front, even though linear internal wave theory predictions were essentially equivalent. Two possible explanations are internal tide generation differences or propagation differences.

In the model, internal tide generation is determined by the baroclinic pressure gradient term. Inspection of time series of the baroclinic pressure gradient terms in the cross-slope velocity momentum equation at a location within the shelf break front ($y = 560$ km) showed significant differences for the two simulations (Figure 9). When the shelf break front was present (solid lines in Figure 9), the baroclinic pressure gradient term was significantly larger. It also fluctuated at the tidal frequency and had a pronounced mean in the lower half of the water column (below $\sigma = 33$). Both this mean and the amplitude of the fluctuation decreased with distance from the bottom (solid lines in Figure 9). The fluctuation of the baroclinic pressure gradient term indicates generation of internal tides with significantly more generation near the bottom. When the shelf break front was absent, the baroclinic pressure gradient term was much smaller, and there was less generation of internal tides (dashed lines in Figure 9). Thus even the slight horizontal density gradient, which existed below 300 m with the presence of this shelf break front, increased the baroclinic pressure gradient term and induced significantly more internal tide generation.

This does not mean that internal tides will not be generated in POM simulations without a front in the domain. Simulations without a front but with stronger stratification (peak $N \geq 3$ cph) show generation of internal tides (not shown) using this modified version of POM, as do other investigators using the original version of POM working in regions with stronger stratification [i.e., Holloway, 1996]. However, generation of internal tides is greatly enhanced in the weak stratification typical of this region by a horizontal pressure gradient associated with a front.

Additionally, K_M for the simulation increased by 1-2 orders of magnitude with the absence of a shelf break front compared to the standard stratification along the upper continental slope, indicating increased dissipation (not shown). With the stratification of the shelf break front, a weaker benthic vertical density gradient existed than without it, and this weaker vertical density gradient increased K_M through its dependence on the Brunt-Väisälä frequency N in the Mellor-Yamada 2.5 level turbulence closure scheme.

Another potential factor for the difference due to the stratification is the propagation of any internal waves, which were generated. The internal wave ray characteristics when the shelf break front was absent (not shown) indicated that the internal tide would not propagate as high in the water column and would stay nearer to the bottom than they do with a shelf break front (part 1, Figure 6a). Consequently, any generated internal waves propagated near or along the bottom, increasing the near-bottom velocity and shear. This focused any modulation in or near the benthic boundary layer. The increased shear would cause a further increase in K_M and dissipation. The net result would be a more uniform velocity profile in the vertical direction and a more pronounced benthic boundary layer. However, the differences due to propagation were smaller than those due to generation.

3.2. Effect of the Location of a Shelf Break Front

To further investigate the effect the location of a shelf break front, a series of simulations were made using the idealized topography described in section 2.4 but with different front locations. The locations used included on the continental shelf, at the continental shelf-slope break, in the middle of the continental slope, and at the bottom of the continental slope. Although simulations with the front on the shelf or over the lower continental slope were unrealistic, they are outer bounds on plausible conditions. A front, in the form of Modified Warm Deep Water (MWDW), was observed 100 km onto the continental shelf [*Foster and Carmack, 1976*]. Continental shelf waves are one of the mechanisms which move shelf break fronts back and forth across the continental shelf-slope break. It is not suggested that continental shelf waves were responsible for the 100 km movement of this front; however, they could have been a contributing factor.

The shelf break position comparison will be made using the cross-slope baroclinic velocities at a time near the peak offshore flow ($t = 45.685$ days) (Figure 10) since they better illustrate the shear in the water column than the major axes of the tidal ellipses. Spectral analysis showed that most of the energy occurred at the M_2 tidal frequency. The exception to this is, of course, the benthic boundary layer, where dissipation increases energy at other frequencies. Since most of the energy was at the tidal frequency, the baroclinic velocity (defined as the difference between the depth-dependent and depth-independent velocities) indicated the vertical variation and shear associated with the M_2 internal tide along with inertial oscillations at that frequency. For clarity on the front location, contours of the density at 0.02 kg m^{-3} intervals were overlaid as dashed lines on the cross-slope baroclinic velocities.

When the front is located in the middle of the continental shelf, there was very little vertical variation in the cross-slope baroclinic velocity even within the front (Figure 10a). The response is very similar to that of the simulation without a shelf break front. Both a thick boundary layer (Figure 10a) and a high K_M existed over the outer continental shelf (Figure 11a). As discussed earlier, there was no horizontal potential density gradient equatorward of ψ_{crit} , and with this weak stratification without a horizontal potential density gradient, internal tide generation was negligible. The lower stratification near the bottom increased K_M and the dissipation (Figure 11a), resulting in a thicker benthic boundary layer (Figure 10a). The shelf break front in this case was located too far onto the continental shelf to have much effect.

When the front was located at the continental shelf-slope break, strong vertical shears were seen in the cross-slope baroclinic velocity, particularly within the front (Figure 10b). The highest velocities occurred just below the permanent pycnocline in the region of the horizontal potential density gradient. The amplitudes were reduced farther down the continental slope. The internal tide energy followed the internal wave ray characteristics, which were parallel to the deeper isopycnals in the front in this case. The deeper isopycnals over the upper continental slope for this scenario were nearly parallel to the bottom due to the averaging used to determine the hydrography. As discussed earlier in section 2, the internal wave ray characteristics were also nearly parallel to the bottom. The higher near-bottom stratification reduced the benthic dissipation from the benthic boundary layer. Propagation of internal tides was primarily offshore, particularly near the surface. K_M peaked near the continental shelf-slope break (Figure 11b), and the benthic boundary layer was much less pronounced for this simulation (Figure 10b). Thus the existence of the shelf break front induced more generation of internal tides and reduced the dissipation.

For both simulations where the front was equatorward of ψ_{crit} the peak vertical variation in the cross-slope baroclinic velocities occurred within the front. In these two cases, there was a significant horizontal potential density gradient across the front below the permanent pycnocline. This horizontal potential density gradient induced internal tide generation through the baroclinic pressure gradient term as discussed earlier. Although the magnitudes of the velocities were reduced, the internal tide response encompassed the entire water column over the continental slope (Figures 10c and 10d), and internal tide propagation occurred along internal wave ray characteristics. Distinct peaks in K_M were present both in the midwater column at the continental shelf-slope break and near the bottom at the edges of the front (Figures 11c and 11d). Reflection of internal tides by ψ_{crit} increased the midwater column K_M through increased vertical shear. The higher deep K_M resulted from the lower N on either side of the front combined with the shear from the internal tides. Although this K_M was dependent on the Mellor-Yamada 2.5 level turbulence closure scheme, it nevertheless indicated the potential for more vertical mixing. Thus the presence and location of a front is important in the generation and propagation of the internal tides in this region and in inducing vertical structure to the horizontal velocities, particularly within the front.

3.3. Effect of Summer Stratification

A simulation was performed with a typical austral summer mixed layer. For summer conditions the hydrography for the upper 100 m was uniform over the entire domain as adapted from observations of K. W. Nicholls (personal communication, 1998) during the Ropex experiment (data locations shown by crosses in part 1, Figure 2b). N peaked at ~ 8 cph at the seasonal pycnocline. With the summer stratification, there was an increase in vertical variation in the major axes of the tidal ellipses (Figure 7b). Profiles of the cross-slope

velocities showed more vertical variation and equatorward propagation of the internal tides than with the standard stratification (Figure 8c compared to Figure 8b). The differences were attributable both to generation and propagation. The deep generation was driven by the horizontal potential density gradients in the lower water column, which were the same for both cases. However, the surface stratification was now strong enough to generate internal tides at the seasonal pycnocline. With the summer stratification, internal tides were trapped in the surface layer, causing them to propagate farther out over the continental slope (Figures 7b and 8c).

4. Topographic Effects

To investigate the sensitivity to slope steepness, a simulation was performed for a transect with a steeper slope (transect B in Figure 1) using austral summer stratification conditions. The depth-independent major axes for the tidal ellipses were slightly smaller with the steeper slope (solid line in Figure 12a) than for transect A (dashed line in Figure 12a). The depth-independent velocities were affected by the outflow at the ice shelf end with a larger outflow associated with smaller velocities. The outflow for transect B was slightly wider than that for transect A, thus the smaller barotropic velocities.

Linear theory predicted that internal tides will be generated over a narrower section of the continental slope (part 1, Figure 5d). The major axes of the tidal ellipses followed this prediction with most of the vertical variation occurring in a narrow band (Figure 12b). Higher values for the major axes extended farther out over the continental slope, indicating increased surface propagation. These major axes peaked deeper in the water column than those for transect A (Figure 12b) because of ψ_{crit} being equatorward of the continental shelf-slope break. This position of ψ_{crit} increased the benthic response; nevertheless, the slope steepness was sufficient for internal tidal generation.

The slopes of transect A and B are typical for the continental slope in the Weddell Sea. Most of the steep slopes lie roughly between the 500 and 1000 m isobaths in the southern and eastern regions. Since proximity to the critical latitude is important for internal tide generation and ψ_{crit} passes through the southern Weddell Sea but not the eastern Weddell Sea, more internal tide generation is predicted in the southern Weddell Sea. For the southern Weddell Sea a histogram of the slope steepness, $\partial H / \partial y$, along the continental slope (defined as water depths between 500 and 3000 m) for the Weddell Sea using the water column thickness of *Robertson et al.* [1998] shows that ~6% of bottom slope has a steepness similar to that of transect A ($\partial H / \partial y \approx 0.022$) and ~10% has a steepness similar to that of transect B ($\partial H / \partial y \approx 0.037$) (Figure 13). These regions could have similar internal tidal fields and vertical structure as those of the transects simulated here depending on their location with respect to ψ_{crit} and the stratification.

5. Implications of Model Results

Mixing and heat fluxes can result either from instabilities due to baroclinic tides and internal waves or from benthic frictional stresses extending into the water column. Although some of the vertical variation in the horizontal velocities is apparent in the major axes of the tidal ellipses, the major axes fail to indicate all of the vertical variation and shear in the horizontal velocities due to the lack of phase information. Comparison of vertical shears in the horizontal depth-dependent velocities averaged over 2 days for three different stratifications schemes, deep water stratification (no shelf break front), winter (shelf break front), and summer (shelf break front), showed strong vertical shears in the horizontal velocities for all three cases (Figure 14). In the case without a shelf break front the vertical shear occurred only in the benthic boundary layer (Figure 14a). With the winter stratification (shelf break front), strong shears occurred both in the benthic boundary layer and in the midwater column in the region of the front just poleward of ψ_{crit} (Figure 14b). The high midwater column vertical shears were a result of equatorward propagation of the internal tide. With the summer stratification, midwater column shears were enhanced, and they extended farther over the continental slope (Figure 14c). It should be noted that these shears were comparable to vertical shears observed nearby (part 1, Table 3) but much less than the maximum observed midwater column shears of $3 \times 10^{-3} \text{ s}^{-1}$ from AnzFlux in the eastern Weddell Sea [*Robertson et al.*, 1995], which were associated with heat fluxes of 20-100 W m^{-2} . The difference was not surprising since the predominant processes are different in the eastern and western portions of the Weddell Sea [*Robertson*, 1999].

Lead formation due to tidal divergence can affect the ocean-atmosphere heat flux, increasing it by as much as 1-2 orders of magnitude [*Maykut*, 1986]. Therefore a lead formation percentage of 1% could potentially double the heat flux from the ocean to the atmosphere.

The lead formation percentage $L_{\%}$ was estimated from the divergence of the depth-dependent velocities at the surface according to

$$L\% = 0.5T\langle\nabla\cdot V\rangle, \quad (2)$$

where T is the tidal period (34,712 s for M_2), $\nabla\cdot V$ is the divergence of the depth-dependent velocity, and angle brackets indicate the standard deviation of the quantity. Since $\partial/\partial x$ is zero due to the two-dimensional application, the along slope velocity makes no contribution to the divergence (i.e., $\nabla\cdot V = \partial U/\partial x + \partial V/\partial y = \partial V/\partial y$). Lead formation percentages were determined for simulations with the winter stratification both with and without a front (Figure 15). When a front was absent, lead formation percentages were quite small, only reaching 1% at the continental shelf slope break (shaded line in Figure 15a with the water depth shown in Figure 15b). However with the winter stratification, the lead percentage was quite high, over 15% at the continental shelf break (black line in Figure 15a). With a front, there was a broad band over the outer continental shelf and upper continental slope where the lead formation percentages were over 1%. This broad band resulted from reflection of the internal tides by the ψ_{crit} . Farther out over the continental slope, smaller bands resulted from constructive and destructive interference of the internal tide as it propagated offshore. It should be noted that addition of other tidal constituents may alter these results, as may three-dimensional horizontal effects, which are absent in this two-dimensional approach.

6. Summary

A modified version of the Princeton Ocean Model was used to investigate sensitivity of the internal tidal dynamics at the M_2 frequency over the outer continental shelf and slope in the southern Weddell Sea to three factors: (1) proximity to the critical latitude, (2) the presence of a shelf break front, and (3) slope steepness.

The internal tidal dynamics were extremely sensitive to all three factors. Generation of internal tides was minimal when the continental shelf-slope break was not in the vicinity of the critical latitude or a shelf break front was not present. Significant internal tide generation occurred only when ψ_{crit} was located near and poleward of the continental shelf-slope break and a shelf break front existed. If ψ_{crit} was located near but equatorward of ψ_{crit} and a shelf break front existed, a set of inertial oscillations in the form of a near-bottom jet developed, and the benthic boundary layer thickness increased.

Stratification was found to be an important factor in influencing both generation and propagation of internal tides and the vertical structure of the horizontal velocities. Without a shelf break front present near the continental slope, few internal tides were generated, and those that were propagated near the bottom, increasing vertical shear in the horizontal velocities and dissipation in the benthic boundary layer. The existence of a front over the upper continental shelf-slope break greatly enhanced the generation of internal tides and/or the development of a near-bottom jet. Although linear internal wave theory provided some insight into the effects of ψ_{crit} , it was inadequate both in estimating the effects of the shelf break front and in predicting the development of the near-bottom jet.

Slope steepness influenced internal tide generation with more generation and more focused generation associated with steeper slopes. The combination of a shelf break front increasing internal tide generation and of ψ_{crit} reflecting the internal tides was found to induce divergence in the horizontal velocities at the surface. These divergences were significant enough to induce lead formation of 1-15% over the continental shelf-slope break. This increase in lead formation could potentially more than double the ocean-atmosphere heat flux.

The greatest significance of the link between the critical latitude and the vertical structure of the horizontal velocities is the application for other regions. This includes not only high-latitude regions such as the Ross and Greenland Seas but also midlatitude regions since the O_1 and K_1 constituents have critical latitudes located at $27^\circ 37'$ and $30^\circ 0'$, respectively. Likewise, the S_2 critical latitude may have a significant effect under the Filchner-Ronne or Ross Ice Shelves.

Even though a typical front location was used for this investigation, continental shelf waves and other mechanisms move the front back and forth across the continental shelf break. Since the relative locations of the front and the critical latitude appear to be crucial for development of vertical shears in the horizontal velocity and for lead formation, further investigation of the interplay of the critical latitude and the position of a front seems warranted. Additionally, investigation of other typical hydrographic conditions would be useful in applying the model results to other locations.

There are several possible extensions of this investigation that would yield further insight into this problem. Increased mixing could result from nonlinearities induced by forcing by more than one tidal constituent. The combination of wind and tidal forcing could also significantly alter the resultant velocity and wave fields. When applying the model to the polar regions, the equation of state should be modified to include thermobaric effects, which are not included at present. An investigation should also include different strengths for the fronts and include scenarios with even more realistic hydrography. Additionally, application of the model in a true three-

dimensional form would simulate the tidal elevations and velocities more accurately and include other processes such as continental shelf waves, which are ignored in the present application.

Acknowledgments. Three anonymous reviewers provided valuable comments on the original manuscript. This study was funded by grant OPP-9896041 from the National Science Foundation (NSF) and UCSIOPO 10075411 from the National Oceanic and Atmospheric Agency (NOAA). The views expressed herein are those of the author and do not necessarily reflect the views of NOAA or any of its subagencies.

References

- Baines, P. G., Internal tides, internal waves, and near-inertial motions, in *Baroclinic Processes on Continental Shelves, Coastal Estuarine Sci. Ser.*, Vol. 3, p. 19-31, AGU, Washington, D. C., 1986.
- Foster, T. D., and E. C. Carmack, Frontal zone mixing and Antarctic Bottom Water formation in the southern Weddell Sea, *Deep Sea Res.*, 23, 301-317, 1976.
- Furevik, T., and A. Foldvik, Stability at M_2 critical latitude in the Barents Sea, *J. Geophys. Res.*, 101, 8823-8837, 1996.
- Holloway, P. E., A numerical model of internal tides with application to the Australian northwest shelf, *J. Phys. Oceanogr.*, 26, 21-37, 1996.
- Huber, B.A., P. A. Mele, W. E. Haines, A. L. Gordon, and V. I. Lutkin, Ice Station Weddell, 1, CTD/hydrographic data, *Tech. Rep. LDEO 94-2*, Lamont-Doherty Earth Obs., Palisades, N. Y., 1994.
- Maykut, G. H., The surface heat and mass balance, in *Geophysics of Sea Ice*, edited by N. Untersteiner, pp. 395-463, Plenum, New York, 1986.
- Middleton, J. H., T. D. Foster, and A. Foldvik, Diurnal shelf waves in the southern Weddell Sea, *J. Phys. Oceanogr.*, 17, 784-791, 1987.
- Robertson, R., Internal tides and baroclinicity in the southern Weddell Sea, 1, Model description, *J. Geophys. Res.*, this issue.
- Robertson, R., Mixing and heat flux mechanisms in the upper ocean in the Weddell Sea, Ph.D. thesis, 173 pp., Oreg. State Univ., Corvallis, Feb. 1999.
- Robertson, R., L. Padman, and G. D. Egbert, Tides in the Weddell Sea, in *Ocean, Ice and Atmosphere: Interactions at the Antarctic Continental Margin, Antarct. Res. Ser.*, Vol. 75, edited by S. S. Jacobs and R. Weiss, pp. 341-369, AGU, Washington, D. C., 1998.
- Robertson, R., L. Padman, M. D. Levine, R. D. Muench, and M. G. McPhee, Internal waves in the eastern Weddell Sea during AnzFlux, paper presented at IAPSO XXI General Assembly, Honolulu, Hawaii, 1995.
- Saint-Guily, B., Sur la propagation des ondes de seconde classe le long d'un talus continental, *C. R. Acad. Sci. Ser. B* 282, 141-144, 1976.

R. Robertson, Lamont-Doherty Earth Observatory, Columbia University, Route 9W, Palisades, NY 10964, USA.
(rroberts@ldeo.columbia.edu)

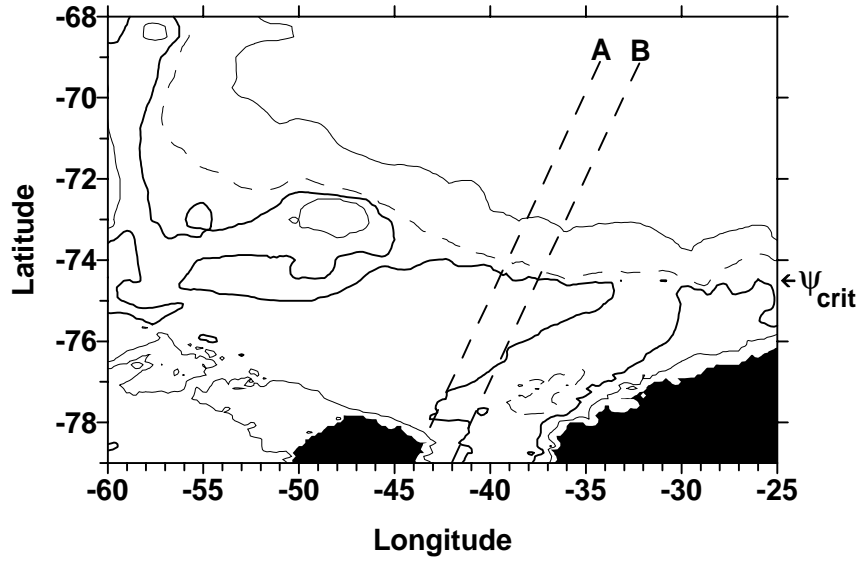


Figure 1. The water column thickness for the southern Weddell Sea contoured at 200, 500 (thick line), 1000 (dashed line), and 3000 m. The location of the transects used for the model domain are shown as dashed lines and labeled A and B. The location of the M_2 critical latitude is indicated by ψ_{crit} along the right axis.

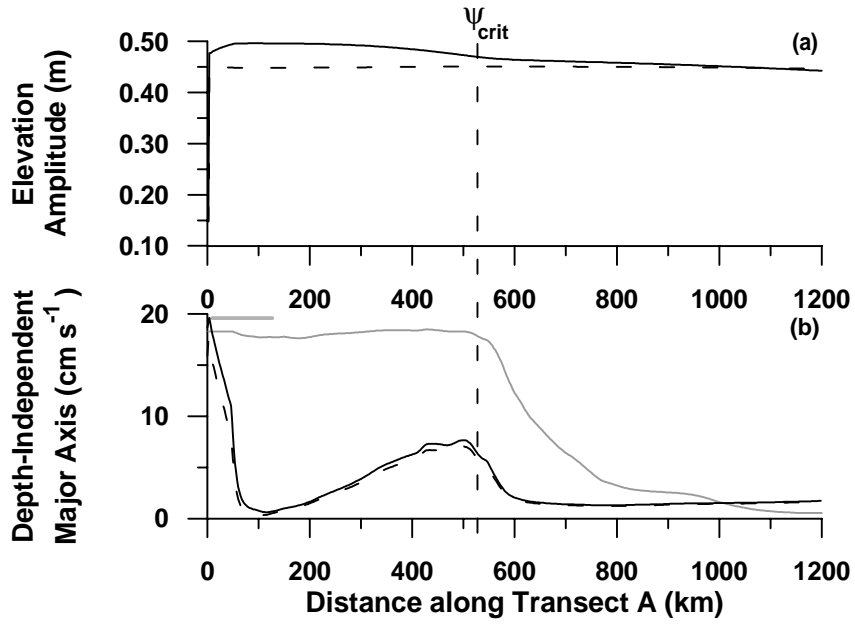


Figure 2. (a) The elevation amplitude from simulations with a stratified ocean with (dashed line) and without (solid line) the M_2 critical latitude crossing through the domain. (b) The major axis of the depth-independent velocities from simulations with (dashed line) and without (solid line) the M_2 critical latitude crossing through the domain. The topography is indicated in Figure 2b by a shaded line. The location of the M_2 critical latitude is denoted with ψ_{crit} in Figure 2a.

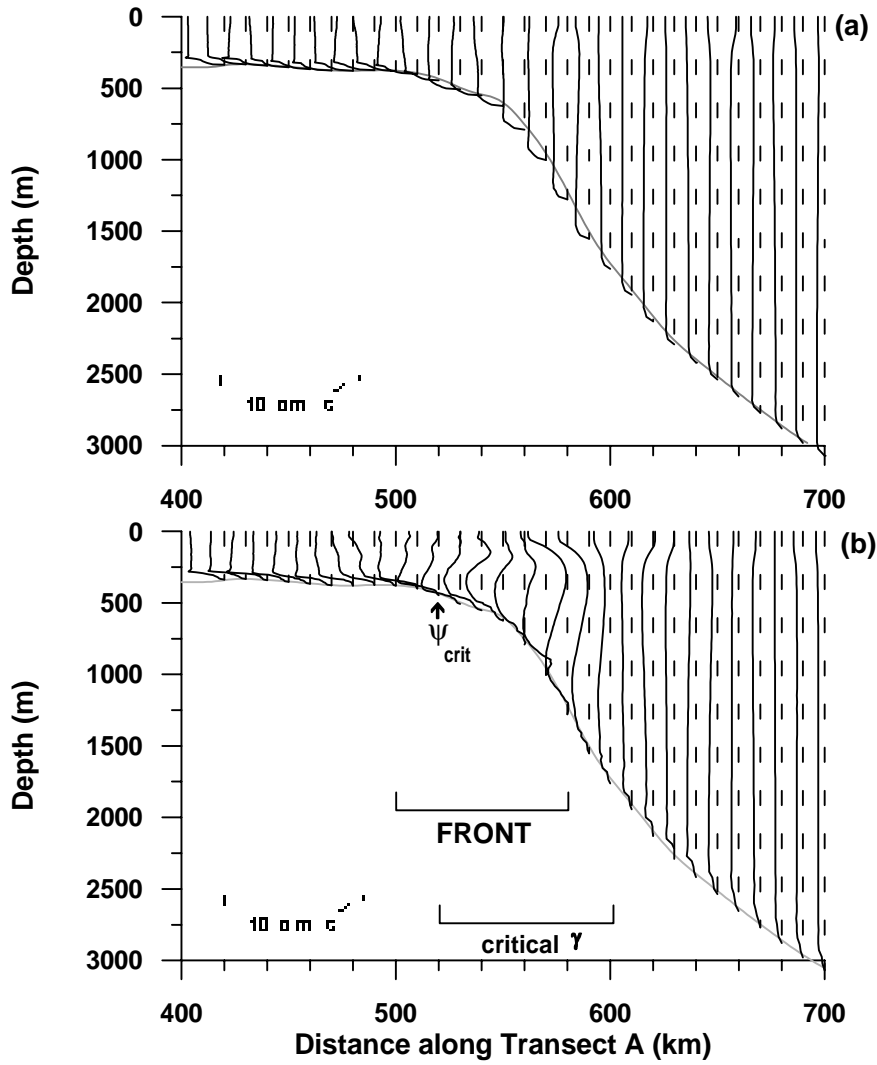


Figure 3. Cross-slope velocity profiles over the continental slope from simulations with stratification for transect A and (a) without and (b) with the critical latitude in the domain (at $t = 45.625$ days). The locations of ψ_{crit} , the shelf break front, and critical γ range are indicated in Figure 3b. Dashed lines representing zero velocity are included for each profile.

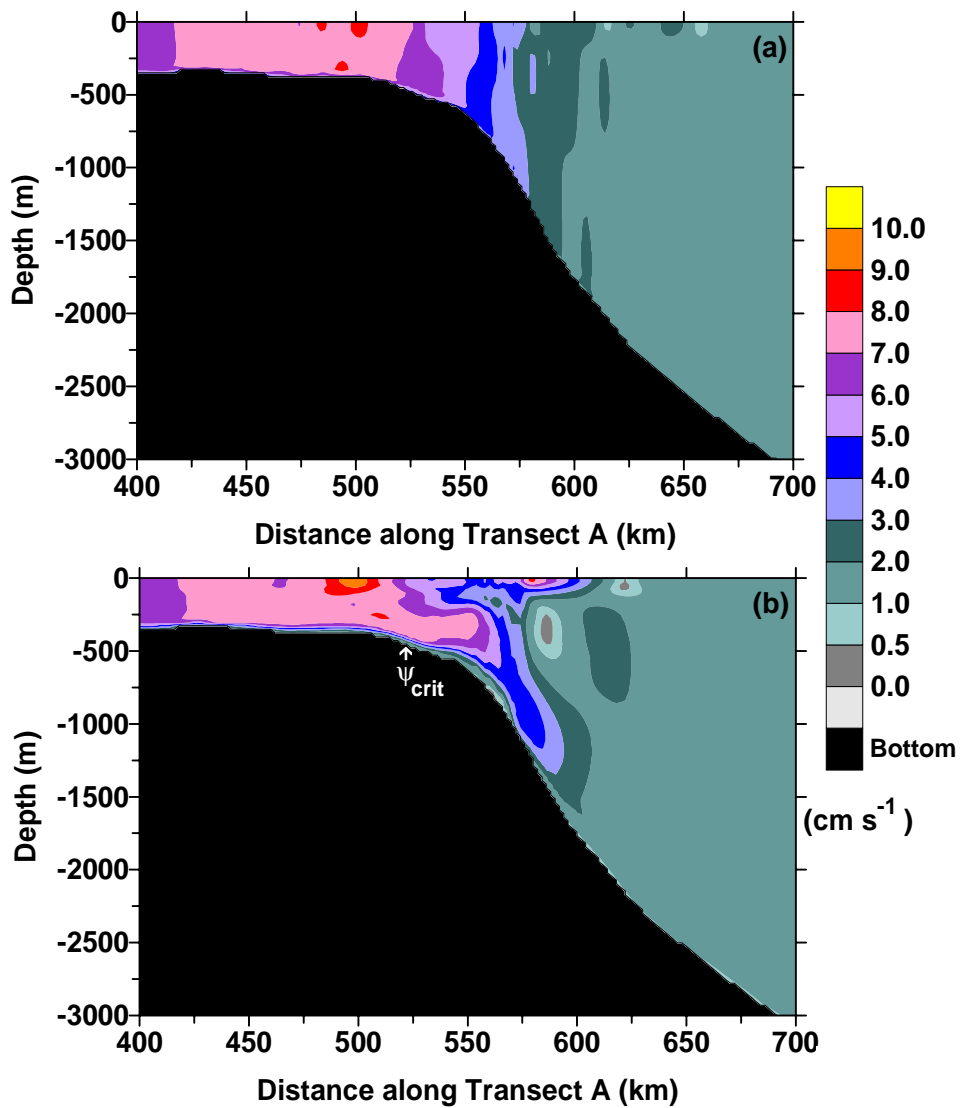


Figure 4. The major axes of the tidal ellipses from simulations with stratification for transect A (a) without and (b) with the critical latitude in the domain. The location of the M_2 critical latitude is denoted in by ψ_{crit} in Figure 4b.

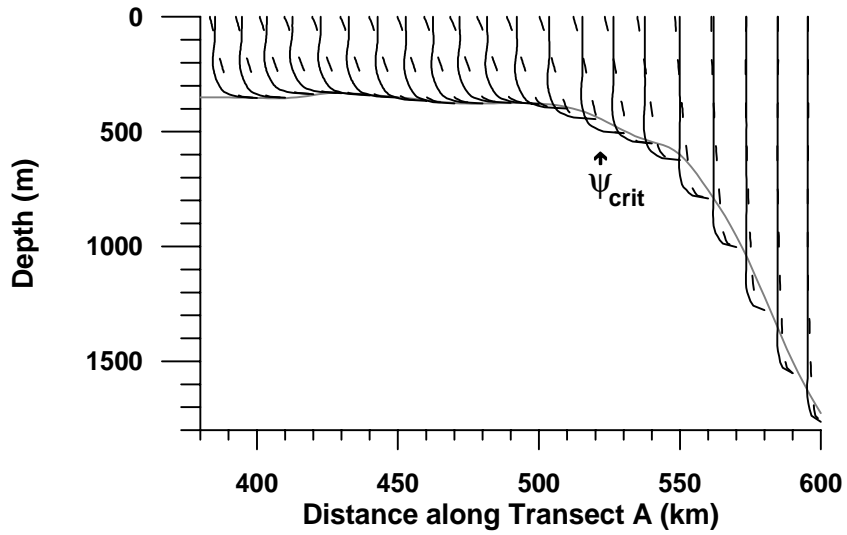


Figure 5. Cross-slope velocity profiles over the continental slope from simulations for transect A without stratification and with (dashed line) and without (solid line) the critical latitude in the domain (at $t = 45.625$ days). The location of the M_2 critical latitude is indicated by ψ_{crit} .

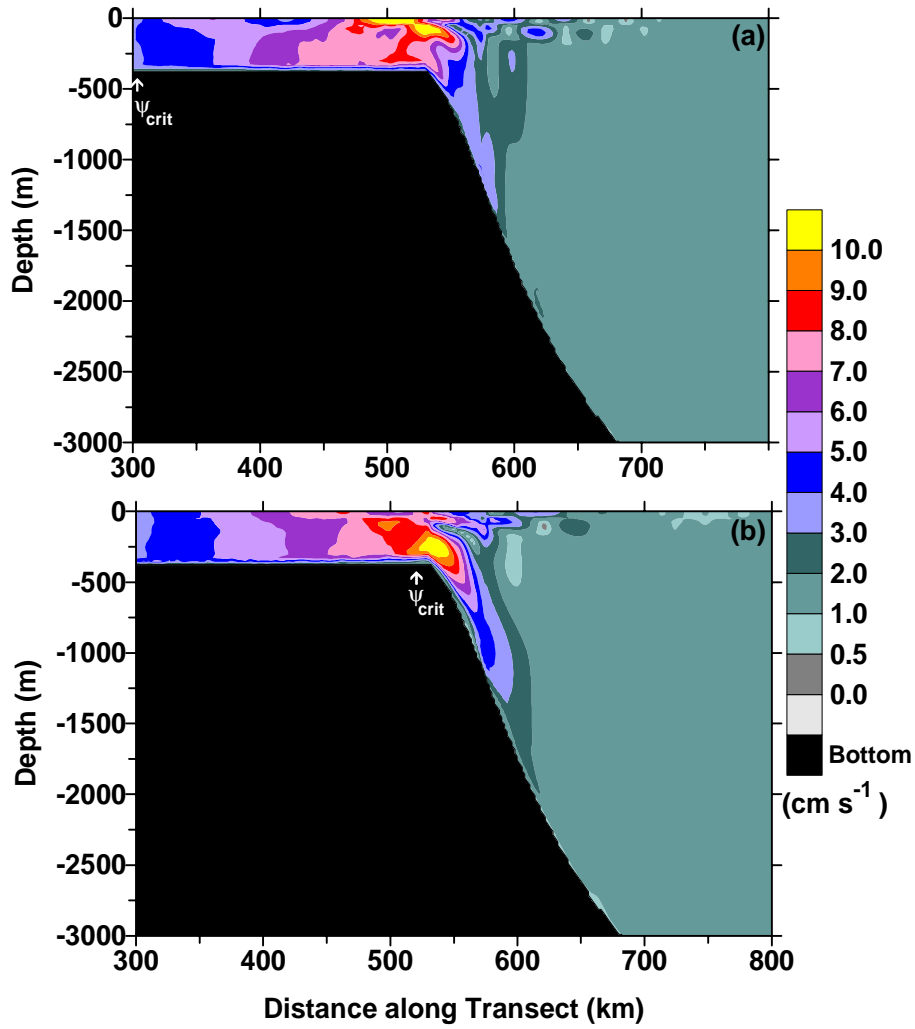


Figure 6. The major axis of the tidal ellipses from simulations with stratification and with the critical latitude located (a) in the middle of the continental shelf, (b) at the upper continental slope, (c) over the middle of the continental slope, and (d) at the lower continental slope. The locations of the critical latitude are denoted in by ψ_{crit} in Figures 6a-6d.

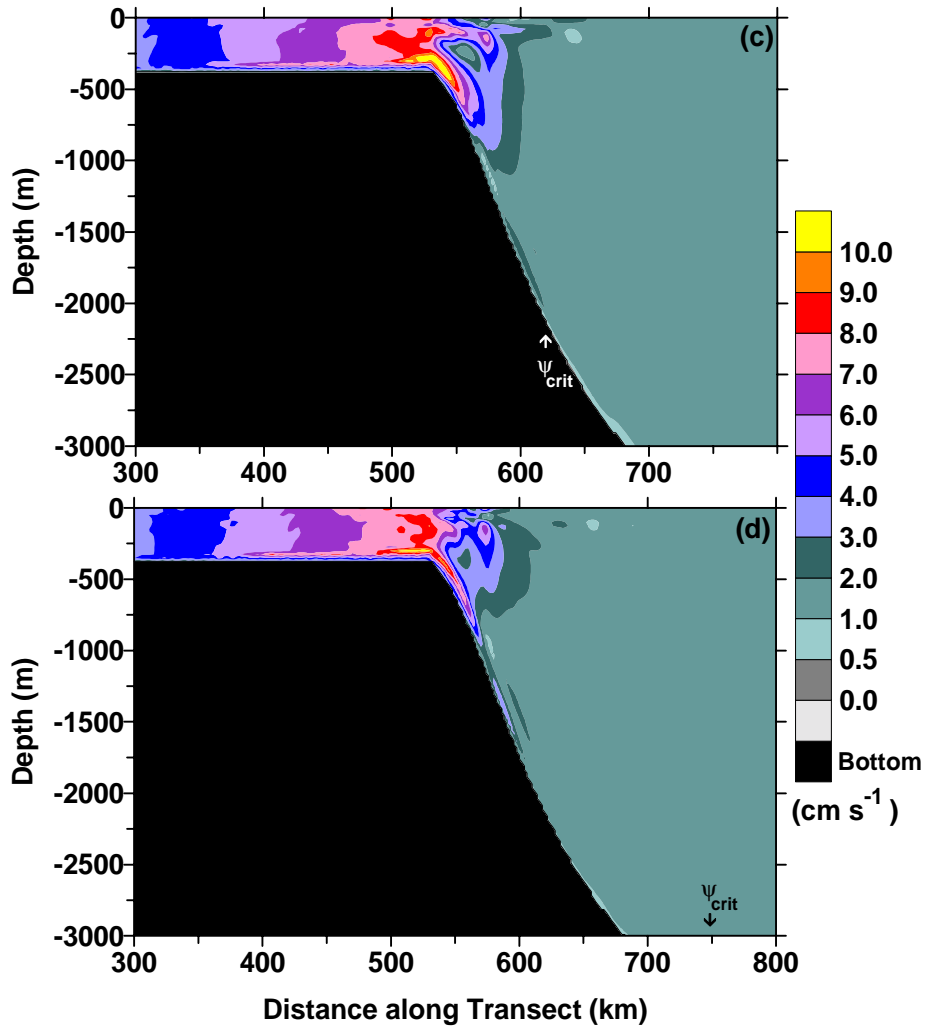


Figure 6. (continued)

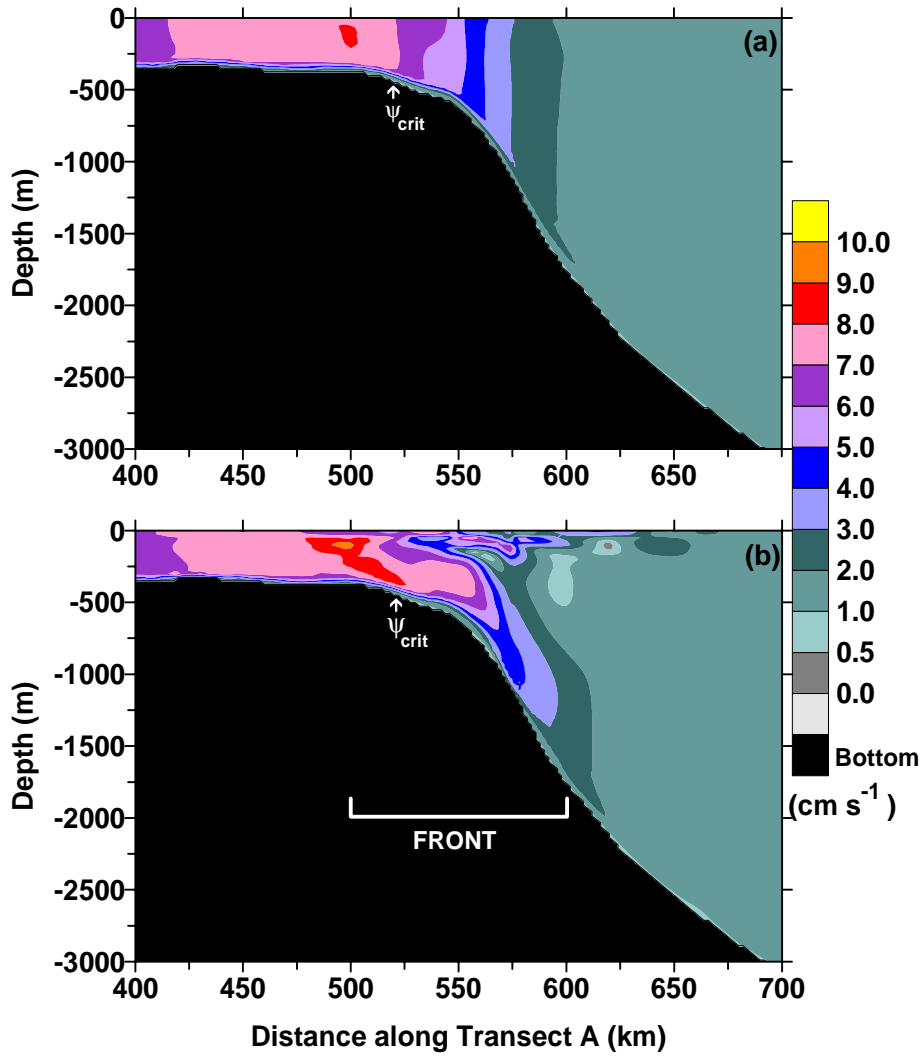


Figure 7. The major axis of the horizontal depth-dependent velocity from simulations for transect A with the critical latitude in the domain and with (a) deep water stratification (no shelf break front) and (b) summer stratification (shelf break front). The locations of the M_2 critical latitude are denoted in Figures 7a and 7b and that of the shelf break front is denoted in Figure 7b.

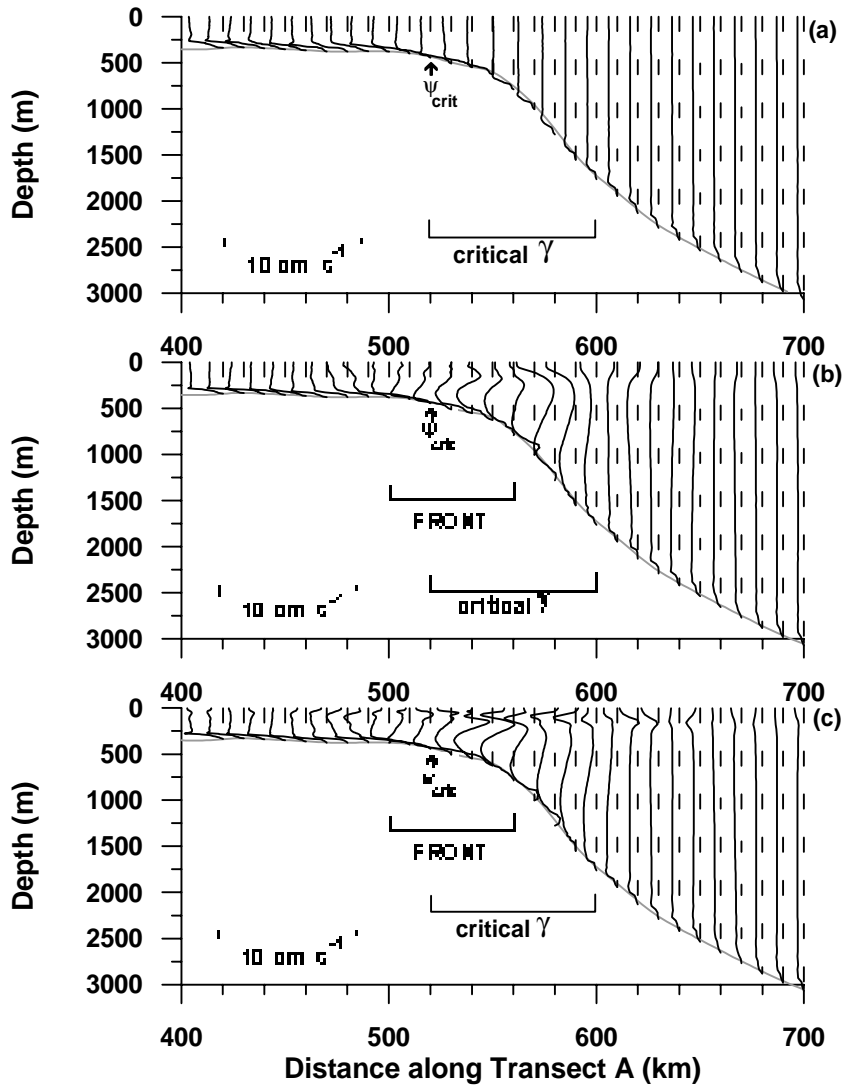


Figure 8. Cross-slope velocity profiles over the upper continental slope for transect A with the critical latitude in the domain from simulations (a) with deep stratification, (b) with the winter stratification, and (c) with summer stratification at $t = 45.625$ days. Dashed lines representing zero velocity are included for each profile.

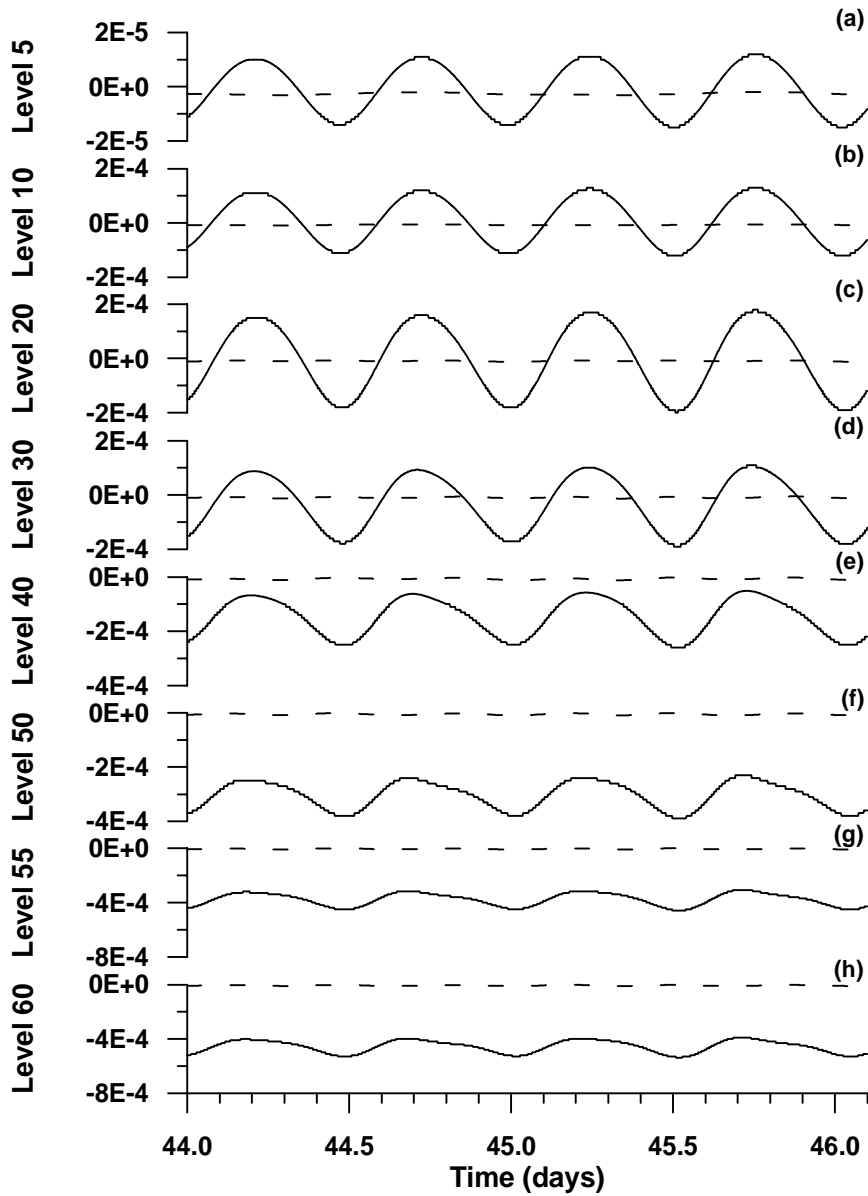


Figure 9. Time series of the baroclinic pressure gradient term at 560 km for the last 2 days of a simulation with the critical latitude in the domain and both winter stratification (shelf break front) (solid line) and deep water stratification (no shelf break front) (dashed line) at sigma levels of (a) 5, (b) 10, (c) 20, (d) 30, (e) 40, (f) 50, (g) 55, and (h) 60.

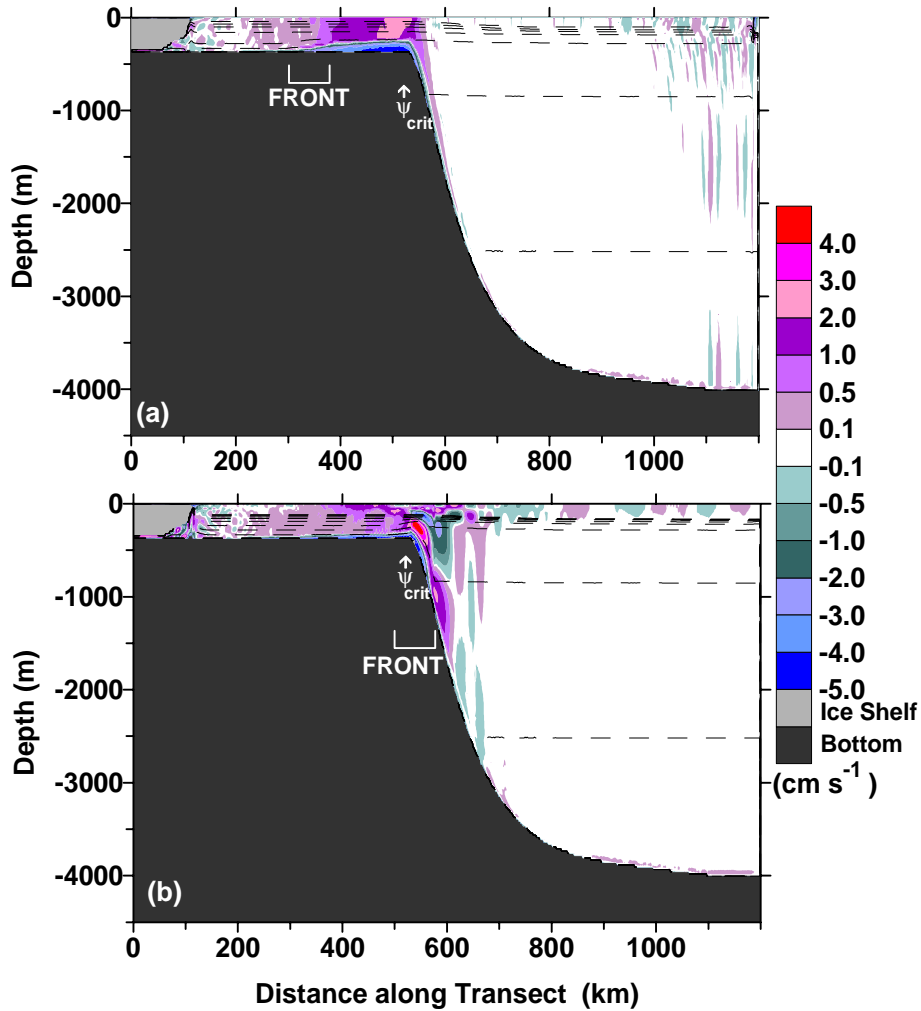


Figure 10. The cross-slope baroclinic velocities at a time near the peak offshore flow ($t = 45.685$ days) for an idealized bottom slope with the critical latitude in the domain when a front is located (a) over the middle of the continental shelf, (b) over the outer continental shelf, (c) over the mid-continental slope, and (d) at the bottom of the continental slope. Contours of the density at 0.02 kg m^{-3} intervals are overlaid as long-dashed lines on the velocity maps. The location of the M_2 critical latitude and the front are indicated in Figures 10a-d.

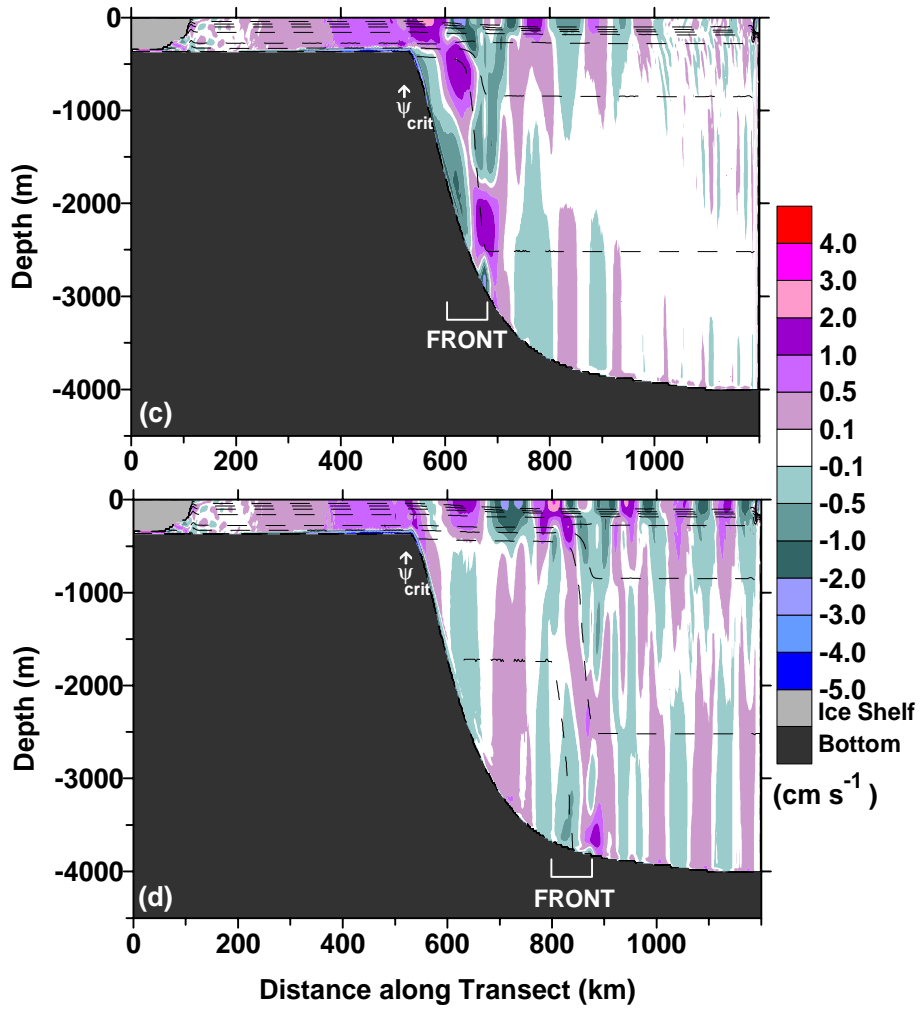


Figure 10. (continued)

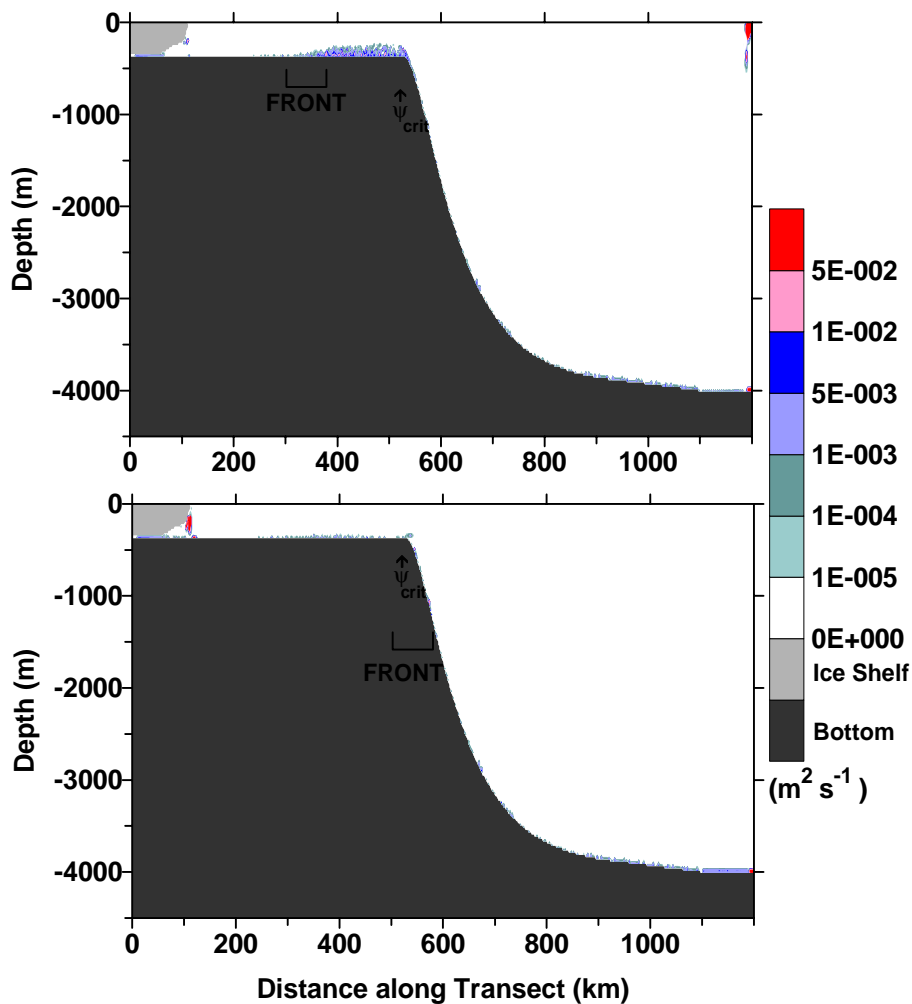


Figure 11. The vertical viscosity coefficient K_M for an idealized bottom slope with the critical latitude in the domain when a front is located (a) over the middle of the continental shelf, (b) over the outer continental shelf, (c) over the midcontinental slope, and (d) at the bottom of the continental slope. The location of the M_2 critical latitude and the front are indicated in Figures 11a-11d.

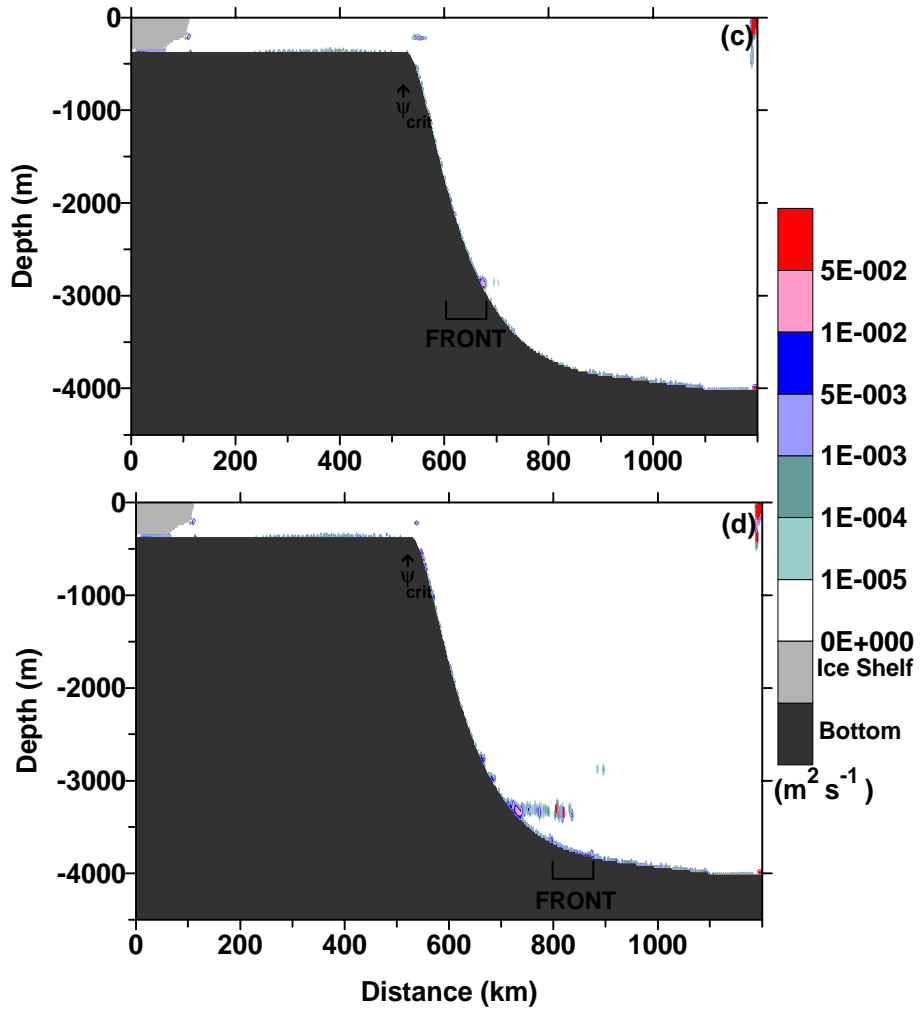


Figure 11. (continued)

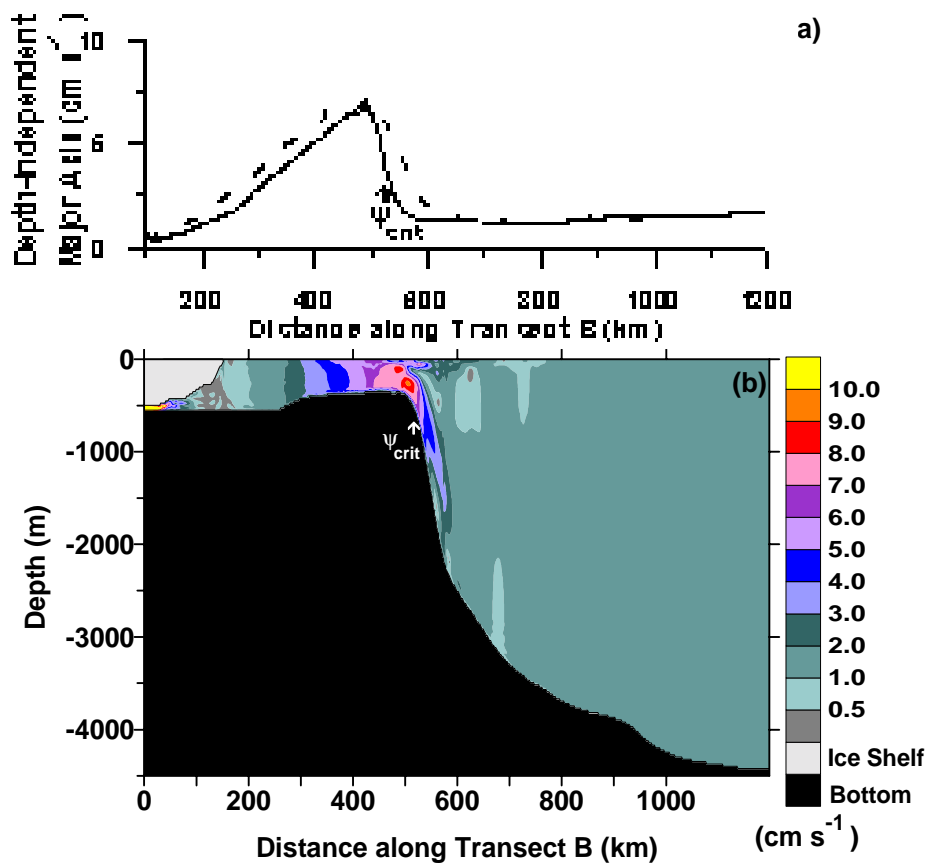


Figure 12. (a) The major axes of the depth-independent velocities for transect A (dashed line) and transect B (solid line) with summer stratification and the critical latitude in the domain. (b) The major axis of the horizontal depth-dependent velocity from simulations for transect B with summer stratification and with the critical latitude located in the domain. The location of the M_2 critical latitude is denoted in by ψ_{crit} in Figures 12a and 12b.

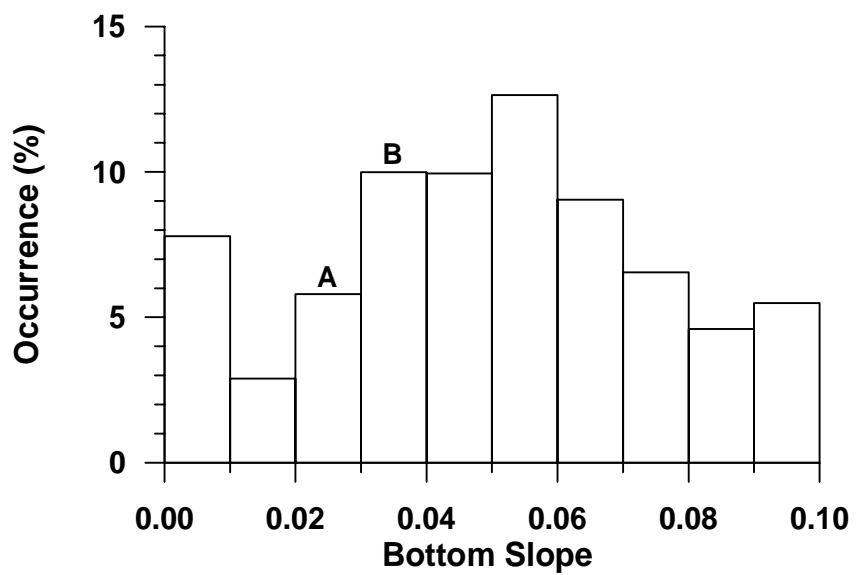


Figure 13. A histogram of the occurrence of the bottom slope steepness with the bins indicated for transects A and B indicated with an A and a B, respectively.

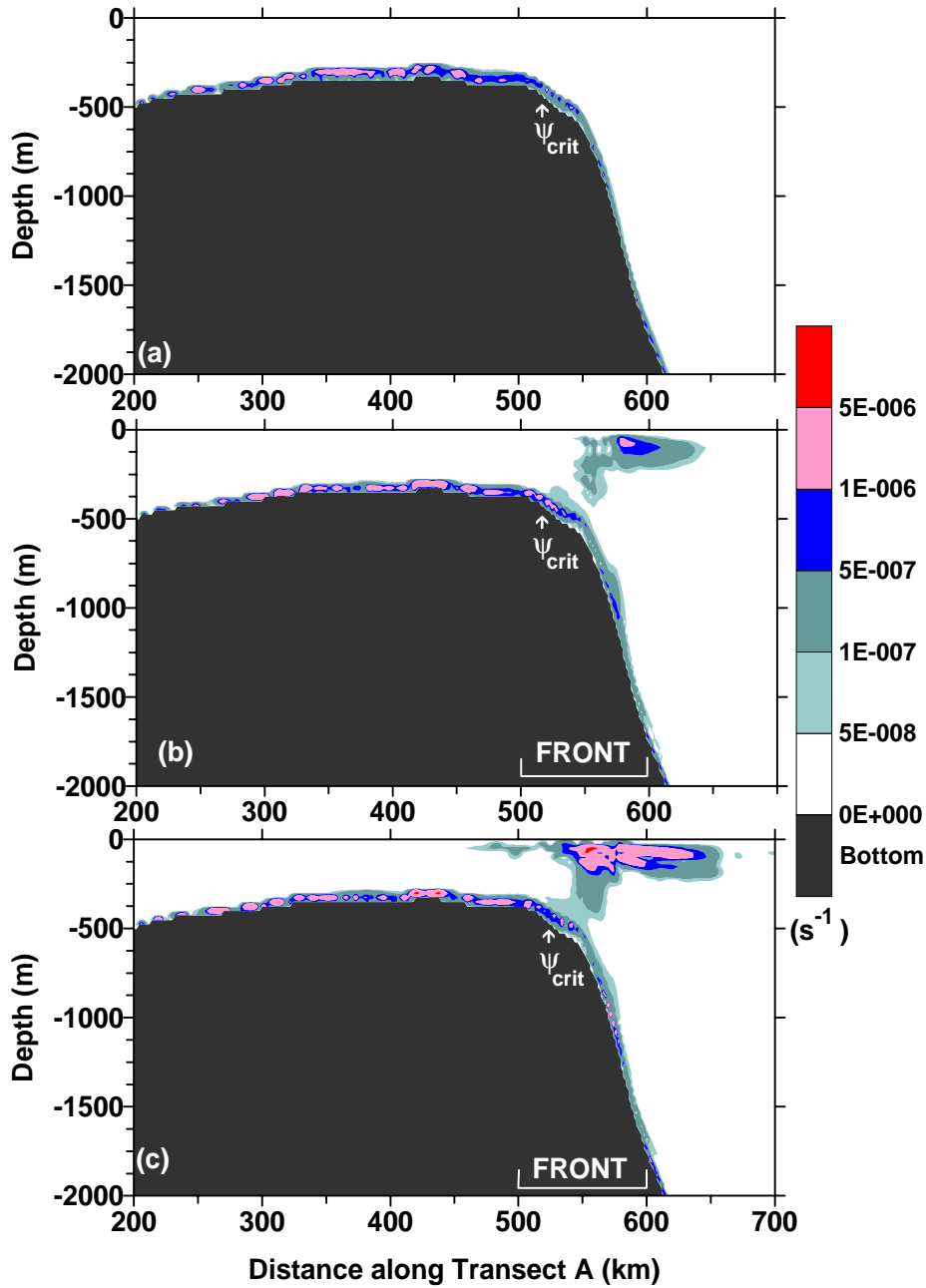


Figure 14. The average vertical shear in the horizontal velocities from simulations for transect A with the critical latitude in the domain and with (a) deep water stratification (no shelf break front), (b) winter stratification (shelf break front), and (c) summer stratification (shelf break front). The locations of the shelf break front and the M_2 critical latitude are indicated in Figures 14a-14c.

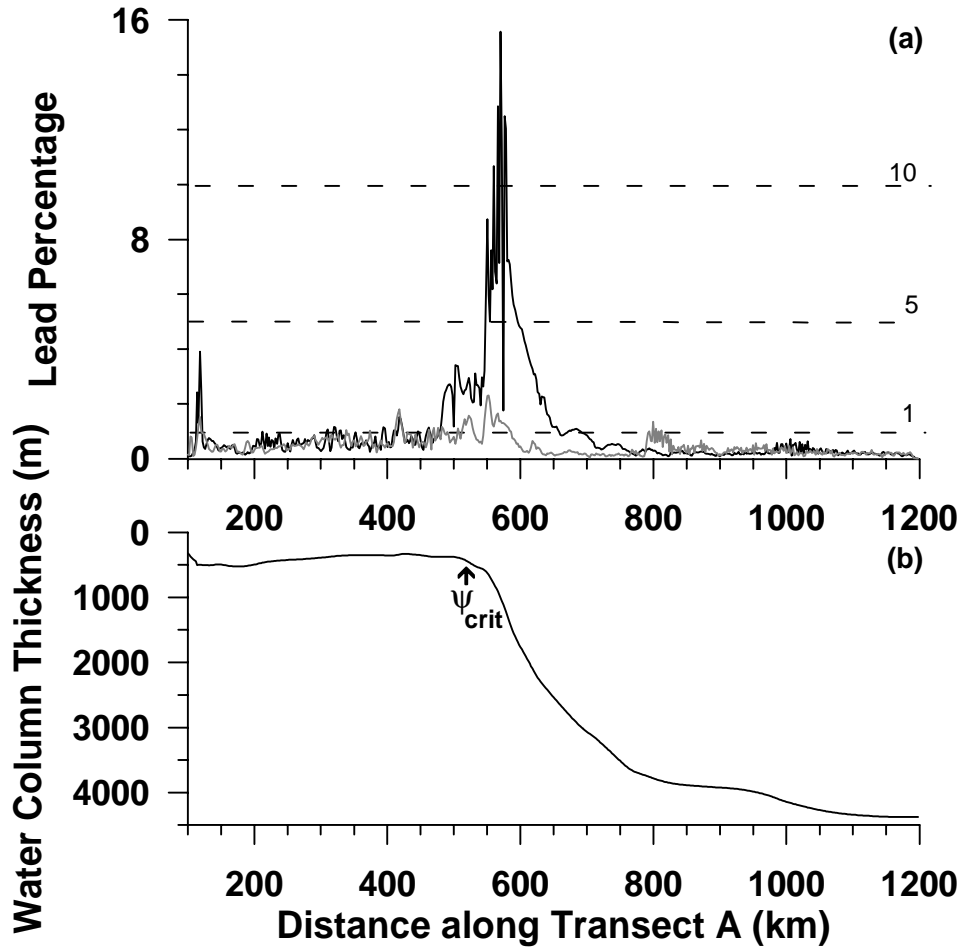


Figure 15. (a) The percentage lead formation as estimated from the tidal divergence at the surface from simulation for transect A with the critical latitude in the domain and without the front (black line) and with the standard stratification (shaded line). (b) The water column thickness over the domain. Dashed lines indicate the percentage levels for 1, 5, and 10%. The location of the M_2 critical latitude is indicated by ψ_{crit} in Figure 15b.